AR-009-172

DSTO-TR-0120

Effects of Case Thickness on the Performance of Underwater Mines

D.A. Jones and E.D. Northeast

DEPARTMENT OF DEFENCE

DEFENCE SCIENCE AND TECHNOLOGY ORGANISATION

Effects of Case Thickness on the Performance of Underwater Mines

D.A. Jones and E.D. Northeast

Weapons Systems Division
Aeronautical and Maritime Research Laboratory

DSTO-TR-0120

ABSTRACT

The effect of case thickness on the performance of underwater mines was investigated both experimentally and computationally using 10 kg charges of H6. The charges were cylindrical in shape and surrounded by either 6 mm or 12 mm thick steel casing. Two bare charges were also fired. Analysis of the experimental pressure transducer records showed that casing thickness had no effect on peak pressure in the far field, but resulted in a 5% increase in shock wave energy compared with an uncased charge. Numerical simulations using both the SIN and DYNA2D codes supported these experimental results. Measurements of the bubble period indicated that the bubble energy for a cased charge was 9% lower than that of an uncased charge.

DEPARTMENT OF DEFENCE

DEFENCE SCIENCE AND TECHNOLOGY ORGANISATION

Published by

DSTO Aeronautical and Maritime Research Laboratory
GPO Box 4331
Melbourne Victoria 3001

Telephone: (03) 626 8111
Fax: (03) 626 8999

AR No. 009-172
January 1995

APPROVED FOR PUBLIC RELEASE

Effects of Case Thickness on the Performance of Underwater Mines

Executive Summary

The underwater performance of explosives has been studied for many years, and the dependence of performance parameters such as shock and bubble energy on charge weight have been well established. Little is known however about the effect that the casing has on the underwater performance of the explosive. This question is of current concern to Navy because of the deployment of the Mk 80 series of bombs in the seamine configuration, and the possibility of a loss in performance due to the relatively thick steel casing of the bombs. To investigate this question a series of experimental firings and numerical simulations have been conducted on scaled generic seamines in both cased and uncased configurations. This report discusses the results of this work in terms of the effect of the thickness of the steel casing on peak shock pressure, and relative shock and bubble energy, for the scaled generic seamines.

The effect of case thickness was investigated both experimentally and computationally using 10 kg charges of the explosive H6. The charges were cylindrical in shape and surrounded by either 6 mm or 12 mm thick steel casing. Two bare charges were also fired. Analysis of the experimental pressure transducer records showed that casing thickness had no effect on peak pressure in the range from 60 to 300 charge radii, but resulted in a 5% increase in shock wave energy compared with an uncased charge. Numerical simulations using both finite difference and finite element hydrocodes supported these experimental results. Our findings with regard to peak pressure and relative shock wave energy are also in good agreement with results found by other recent experimental and numerical investigations. Measurements of the bubble period however indicated that the bubble energy for a cased charge was 9% lower than that of an uncased charge.

Our results indicate that for damage mechanisms due to peak pressure or shock wave energy the relatively thick casing of the Mk 80 series of bombs will not result in any degradation of performance, and may even result in enhanced damage due to shock wave effects. The situation with regard to damage by bubble effects is less clear however, and may at worst result in a 9% reduction in performance, independent of the mass to charge ratio.

Authors

D.A. Jones
Weapons Systems Division

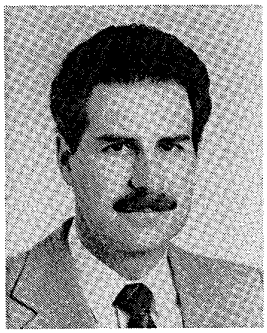

David Jones graduated from Monash University in 1972 with a BSc (Hons). He obtained his PhD from Monash in 1976. His thesis was titled "Anisotropic diffusion in the Townsend-Huxley experiment". After working at Strathclyde University, London University and the University of New South Wales he joined AMRL in 1983. He has worked on the numerical modelling of shaped charge warheads and slapper detonator devices. From February 1987 to May 1988 he was a Visiting Scientist at the Laboratory for Computational Physics and Fluid Dynamics at the Naval Research Laboratories in Washington DC. While there he worked on advanced computational fluid dynamics.

E. Northeast
Weapons Systems Division

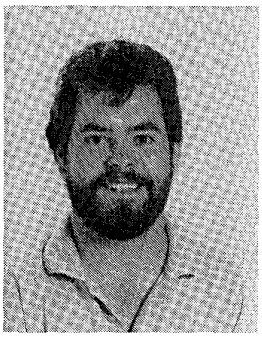

Eric Northeast graduated with a BSc in Computer Science/Physics in 1989 from Chisholm Institute of Technology. He joined AMRL in 1982, where he worked in the areas of hydro-code modelling, slapper detonator fuze research and is currently managing computing in the Weapons Systems Division, AMRL.

Contents

1. Introduction

The underwater performance of explosives has been studied for many years and the dependence of performance parameters such as shock and bubble energy on charge weight have been well established [1]. However, apart from the recent paper by Takahashi et al. [2], little is known about the effect that the explosive casing has on the underwater performance of the explosive. This question is of current concern to Navy because of the deployment of the Mk 80 series of bombs in the seamine configuration and the possibility of a loss in performance due to the relatively thick steel casing of the bombs. To investigate this question a series of experimental firings and numerical simulations have been conducted on scaled generic seamines in both cased and uncased configurations. This report discusses the results of this work in terms of the effect of the thickness of the steel casing on peak shock pressure and relative shock and bubble energy for the scaled generic seamines. We then use these results to comment on the expected performance of the Mk 80 series of bombs when used in the seamine configuration.

2. Field Trial Experiments

2.1 Charge Design and Fabrication

Six experimental charges consisting of 10 kg of H6 in the shape of square cylinders (height equal to diameter = 194 mm) were designed and used for this work. The charges were fired at Epping Quarry, Melbourne, and restrictions at the firing site imposed an upper limit of 25 kg for each charge. The smaller weight of 10 kg was used because of the difficulty in physically handling larger sized charges. No cranes were available at the field site, and the combined weight of charge and casing for the thicker cases was close to 30 kg. The Mk 80 series of bombs has a length to diameter ratio of approximately 5 to 1. It was impractical to reproduce this ratio in the experimental charges and so the square cylinder shape was chosen to reduce directionality effects. One of the advantages of this approach was that the results could be compared with previous experimental results for H6 obtained with spherical charges [3].

Two of the cylinders were fired as bare charges (Events 1 and 2), while the remaining cylinders were confined by either 6 mm (Events 3 and 4) or 12 mm (Events 5 and 6) thick steel casing. The nominal case thickness for most of the Mk 82 bomb is approximately 12 mm, while the 6 mm thick casing represents a typical thickness for a thin walled munition (eg. an 81 mm mortar, which has an average case thickness of 5.5 mm). The steel cases were made from existing steel tubing. A base plate was welded to the bottom of each cylinder, and the top plate was fastened with twelve "Unbrako" case hardened steel screws. Three pieces of angle iron were attached to the sides of the charge and a hole was drilled through the riser so that D-shackles could be attached to the charge. Chains were then threaded through the D-shackles so that the

charge assembly could be lowered into the water. The bare charges were simply placed into plastic mesh "onion" bags for attachment to the lowering assembly.

A diagram of the case assembly is shown in Figure 1. The original intention was to include a hole in the centre of the upper plate for the detonator cord, but during manufacture of the case assembly it was realized that this would lead to problems in correctly locating both the booster and the channel for the detonator cord during the filling operation. To overcome this problem a hole was drilled in the centre of the bottom plate before welding to the cylinders. A wax spigot was then placed over the hole and used to form a channel for the detonator cord. This made the filling operation easier, but created problems during deployment of the charge because the excessive weight of the charge assembly (up to 30 kg) and the positioning of the detonator cord made the charge very awkward to handle, and there was a danger that the cord would inadvertently come into contact with some of the rocky outcrops along the side of the quarry. A simple solution for any further tests of this type would be to weld lifting lugs to the base plate initially, rather than using the three pieces of angle iron that were attached by the steel screws.

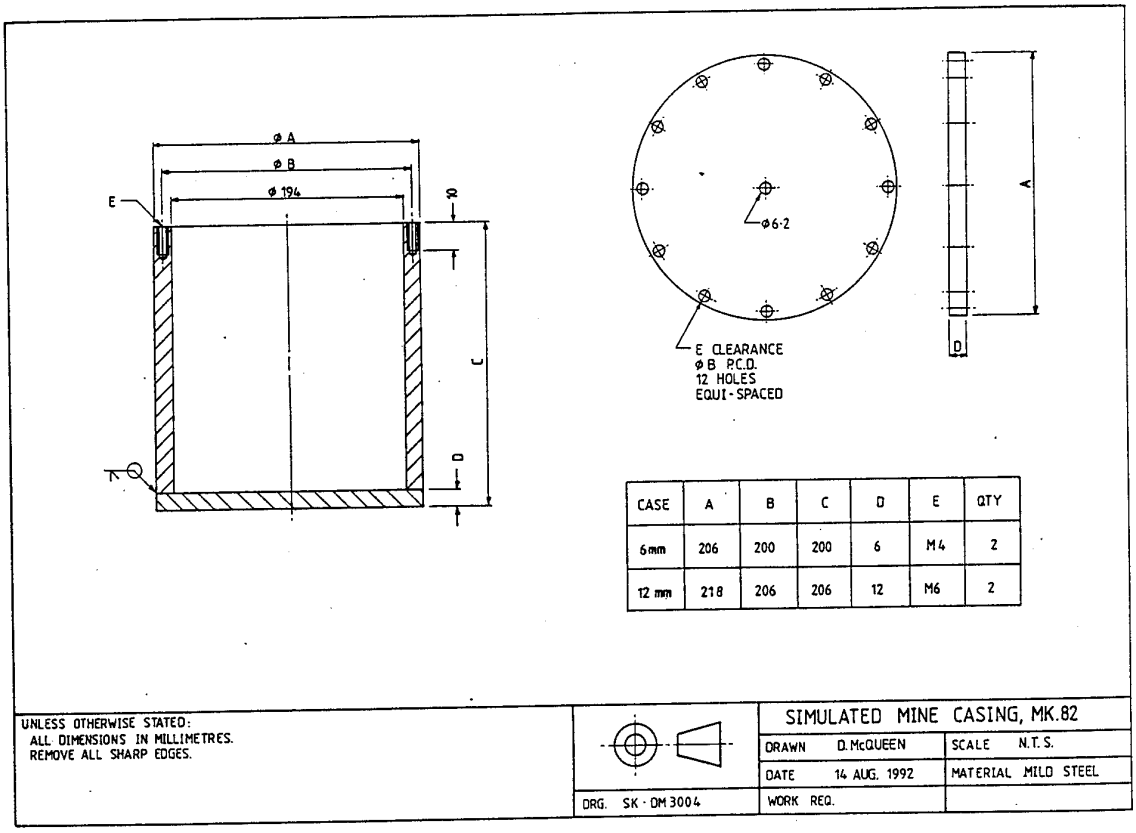

CASE	A	B	C	D	E	QTY
6mm	206	200	200	6	M4	2
12 mm	218	206	206	12	M6	2

Figure 1: Dimensions of the steel cases.

A 100 g cylindrical pentolite booster was used to initiate each charge. These were located in the centre of each charge and were placed in position as the H6 was cast directly into the steel cylinders. The bare charges were also cast into the steel cylinders as it was found that very small amounts of shrinkage occurred, and this allowed the H6 to be eased out of the cylinders after cooling. The shrinkage was quite minimal however and did not effect either the performance or deployment of the cased charges.

2.2 Pressure Transducer Arrays

An array of ten pressure transducers was used to obtain pressure-time profiles at various distances from the charges. Figure 2 shows the relative positions of the charge and pressure transducers. Two steel cables spanned the quarry and the charge was suspended beneath a flying fox which was attached to one of these cables. Nine of the pressure transducers were hung from the second cable at various distances from the charge, and the tenth pressure transducer (the one closest to the charge) was hung from the first cable. All pressure transducers and each charge were deployed 8 m below the surface. The pressure transducers were PCB 138 A05 type containing a tormaline crystal sensing element. Results were recorded directly onto an 80 kHz analogue bandwidth tape recorder.

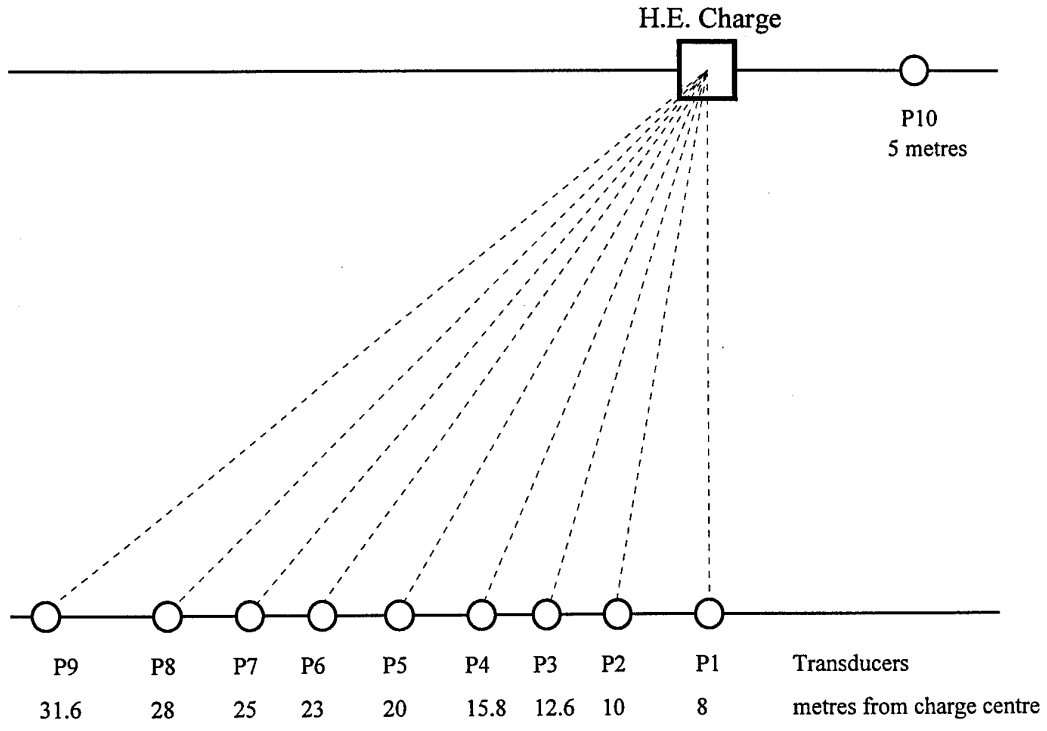

Figure 2: Schematic of charge deployment and pressure transducer locations.

2.3 Fragment Throw

Previous MRL firings at Epping Quarry have always used uncased charges, and so the fragmentation hazard from the steel cased charges used in this study had to be considered. The charge to mass (C/M) ratios for the 6 mm and 12 mm thick casing charges were 1.128 and 0.566 respectively. The CONWEP code [4] was used to calculate typical fragment mass and initial fragment velocities of 7.5 grams and 2250 m/s for the 6 mm casing, and 25 grams and 1750 m/s for the 12 mm casing. Steel cased charges with similar C/M ratios have been tested at the MRL fragmentation pit and the Puckapunyal fragmentation facility and smaller fragments (approximately half the mass) with similar velocities were rapidly retarded in approximately 1.2 metres of water [5]. Therefore it was estimated that even large fragments of 25 grams would have no velocity after travelling through approximately 2 metres of water. This is well below the 8 metre depth at which the charge was fired, and hence it was concluded that there would be zero probability of the high velocity fragments reaching the water surface and creating a hazard. The possibility of the fragments reaching the surface by first being "carried" by the gas bubble as it expanded and then propagating to the water surface was also discounted because a 10 kg charge of H6 explosive would produces a gas bubble of only 3 metres diameter [6], which still leaves 5 metres of water between the edge of the gas bubble and the water surface.

Another scenario which was considered was that fragments could be thrown into the air by the water column as it broke the surface. When the explosive gas bubble collapses a water column travelling at approximately 70 m/s will be produced. Under extreme situations it would be possible for fragments above the gas bubble to be trapped in this water column and then thrown into the air as the water column disperses. Results from Jenks et al. [7] indicate that the horizontal range for a 25 gram fragment thrown at a 30 degree angle would be 95 metres. Distances of this magnitude are highly unlikely however as the fragment is more likely to travel near vertically. If the fragment was thrown at an angle of 70 degrees then the range would be only 49 metres. All personnel were located at considerably greater distances from the charge during actual firing, and so it was concluded that the fragmentation of the steel casing did not provide any additional hazards.

3. Experimental Results

The peak pressure, impulse, energy flux density, bubble period, time of arrival, and other useful data measured at each of the ten gauge locations for events one through six are tabulated in Tables 1 and 2. Before examining the effect of case thickness on these performance parameters we first analyse the data for the bare charges and compare the results with previous experimental work on H6 [3].

Table 1:

Event 1

Gauge	Peak Pressure		5θ	Impulse	E.F.D.	Shock	Data File	Calibration	T/A	R	B.P.
	(psi)	(MPa)	(μs)	(kPa.s)	(m.kPa)	Factor	Name	File Name	(ms)	(m)*	(ms)
P1	2090	14.41	1332.5	4.706	18.674	0.47	SCEP1E1.D01	D2P1.CAL	5.122	7.54	463.55
P2	1739	11.99	1469.5	4.491	14.884	0.42	SCEP2E1.D01	D2P2.CAL	6.061	8.93	463.40
P3	1403	9.67	1285	3.103	8.064	0.309	SCEP3E1.D01	D2P3.CAL	7.661	11.30	462.85
P4	1030	7.10	1497.5	2.821	5.555	0.257	SCEP4E1.D01	D2P4.CAL	9.697	14.28	462.70
P5	793	5.47	1565	2.165	3.149	0.193	SCEP5E1.D01	D2P5.CAL	12.51	18.43	462.35
P6	624	4.30	1348	1.523	1.822	0.147	SCEP6E1.D01	D2P6.CAL	14.55	21.94	462.40
P7	651	4.49	1442.5	1.658	2.056	0.156	SCEP7E1.D01	D2P7.CAL	15.84	23.34	462.20
P8	880	6.07	597.5	1.113	1.454	0.131	SCEP8E1.D01	D2P8.CAL	17.81	26.24	462.55
P9	541	3.73	1855	1.701	1.716	0.143	SCEP9E1.D01	D2P9.CAL	20.37	30.01	461.90
P10	2717	18.73	1317.5	6.507	33.543	0.63	SCEP10E1.D01	D2P10.CAL	4.112	6.06	464.15

Event 2

Gauge	Peak Pressure		5θ	Impulse	E.F.D.	Shock	Data File	Calibration	T/A	R	B.P.
	(psi)	(MPa)	(μs)	(kPa.s)	(m.kPa)	Factor	Name	File Name	(ms)	(m)*	(ms)
P1	2090	14.41	1335	4.744	19.155	0.476	SCEP1E2.D01	D2P1.CAL	5.120	7.54	465.20
P2	1758	12.12	1449	4.561	15.437	0.428	SCEP2E2.D01	D2P2.CAL	6.009	8.85	464.90
P3	1421	9.80	1240	2.894	7.515	0.298	SCEP3E2.D01	D2P3.CAL	7.602	11.20	463.90
P4	1057	7.30	1497	2.81	5.531	0.256	SCEP4E2.D01	D2P4.CAL	9.619	14.17	463.40
P5	812	5.60	1441	2.101	3.174	0.194	SCEP5E2.D01	D2P5.CAL	12.44	18.32	463.90
P6	1386	9.56	260	0.752	1.673	0.141	SCEP6E2.D01	D2P6.CAL	14.48	21.33	464.00
P7	663	4.57	1477	1.658	2.053	0.156	SCEP7E2.D01	D2P7.CAL	15.70	23.12	463.30
P8	998	6.88	406	0.795	1.166	0.118	SCEP8E2.D01	D2P8.CAL	17.72	26.10	463.60
P9	534	3.68	1605	1.594	1.631	0.139	SCEP9E2.D01	D2P9.CAL	20.30	29.90	464.50
P10	2833	19.53	1308	6.485	33.917	0.634	SCEP10E2.D01	D2P10.CAL	4.196	6.180	465.10

Event 3

Gauge	Peak Pressure		5θ	Impulse	E.F.D.	Shock	Data File	Calibration	T/A	R	B.P.
	(psi)	(MPa)	(μs)	(kPa.s)	(m.kPa)	Factor	Name	File Name	(ms)	(m)*	(ms)
P1	2168	14.94	1416	4.726	19.966	0.486	SCEP1E3.D01	D3P1.CAL	5.122	7.54	449.10
P2	1769	12.20	1487	4.35	15.454	0.428	SCEP2E3.D01	D3P2.CAL	6.031	8.88	448.00
P3	1392	9.60	1418	3.212	8.453	0.316	SCEP3E3.D01	D3P3.CAL	7.627	11.23	447.5
P4	1067	7.36	1713	3.046	6.02	0.267	SCEP4E3.D01	D3P4.CAL	9.639	14.20	449.10
P5	800	5.52	1473	2.051	3.163	0.194	SCEP5E3.D01	D3P5.CAL	12.47	18.37	448.50
P6	1281	8.83	430	1.101	2.52	0.173	SCEP6E3.D01	D3P6.CAL	14.51	21.37	448.60
P7	637	4.39	1550	1.724	2.132	0.159	SCEP7E3.D01	D3P7.CAL	15.79	23.26	448.40
P8	469	3.23	1645	1.537	1.354	0.127	SCEP8E3.D01	D3P8.CAL	17.77	26.18	448.70
P9	518	3.57	1814	1.708	1.708	0.142	SCEP9E3.D01	D3P9.CAL	20.33	29.95	448.60
P10	4179	28.82	1624	7.702	43.271	0.716	SCEP10E3.D01	D3P10.CAL	4.141	6.10	448.70

* Note: Slant range (R) is derived from the Time of Arrival (T/A) multiplied by the acoustic water velocity (=1473 m/s; based on temperature and salinity measurements).

Table 2:

Event 4

Gauge	Peak Pressure		5θ	Impulse	E.F.D.	Shock	Data File	Calibration	T/A	R	B.P.
	(psi)	(MPa)	(μs)	(kPa.s)	(m.kPa)	Factor	Name	File Name	(ms)	(m)*	(ms)
P1	2168	14.94	1411	4.83	20.332	0.491	SCEP1E4.D01	D3P1.CAL	5.090	7.50	448.70
P2	1806	12.45	1529	4.61	16.513	0.442	SCEP2E4.D01	D3P2.CAL	6.005	8.85	448.60
P3	1374	9.48	1364	3.041	8.12	0.31	SCEP3E4.D01	D3P3.CAL	7.601	11.20	448.50
P4	1085	7.48	1614	2.929	5.933	0.265	SCEP4E4.D01	D3P4.CAL	9.624	14.18	448.40
P5	818	5.64	1564	2.195	3.351	0.199	SCEP5E4.D01	D3P5.CAL	12.45	18.33	448.30
P6	-----	-----	-----	-----	-----	-----	SCEP6E4.D01	D3P6.CAL	14.49	21.35	448.40
P7	663	4.57	1505	1.691	2.132	0.159	SCEP7E4.D01	D3P7.CAL	15.78	23.24	447.80
P8	-----	-----	-----	-----	-----	-----	SCEP8E4.D01	D3P8.CAL	17.79	26.16	448.50
P9	548	3.78	1715	1.66	1.709	0.142	SCEP9E4.D01	D3P9.CAL	20.32	29.94	448.60
P10	3415	23.54	1679	8.004	42.613	0.711	SCEP10E4.D01	D3P10.CAL	4.152	6.06	447.80

Event 5

Gauge	Peak Pressure		5θ	Impulse	E.F.D.	Shock	Data File	Calibration	T/A	R	B.P.
	(psi)	(MPa)	(μs)	(kPa.s)	(m.kPa)	Factor	Name	File Name	(ms)	(m)*	(ms)
P1	2205	15.20	1370	4.415	19.386	0.479	SCEP1E5.D01	D3P1.CAL	5.646	8.32	449.70
P2	1732	11.94	1676	4.707	15.455	0.428	SCEP2E5.D01	D3P2.CAL	6.816	10.04	450.20
P3	1383	9.54	1384	2.994	7.887	0.306	SCEP3E5.D01	D3P3.CAL	8.481	12.49	449.60
P4	1031	7.11	1820	3.063	5.872	0.264	SCEP4E5.D01	D3P4.CAL	10.60	15.62	450.00
P5	808	5.57	1796	2.369	3.453	0.202	SCEP5E5.D01	D3P5.CAL	13.38	19.71	449.50
P6	609	4.20	1805	1.803	2.028	0.155	SCEP6E5.D01	D3P6.CAL	15.47	22.79	449.60
P7	615	4.24	2007	1.881	2.138	0.159	SCEP7E5.D01	D3P7.CAL	16.80	24.75	449.30
P8	-----	-----	-----	-----	-----	-----	SCEP8E5.D01	D3P8.CAL	18.76	27.63	449.50
P9	536	3.695	2081	1.773	1.777	0.145	SCEP9E5.D01	D3P9.CAL	21.33	31.42	449.30
P10	2854	19.68	1647	7.833	41.787	0.704	SCEP10E5.D01	D3P10.CAL	4.488	6.61	449.20

Event 6

Gauge	Peak Pressure		5θ	Impulse	E.F.D.	Shock	Data File	Calibration	T/A	R	B.P.
	(psi)	(MPa)	(μs)	(kPa.s)	(m.kPa)	Factor	Name	File Name	(ms)	(m)*	(ms)
P1	2186	15.07	1531	5.237	22.207	0.513	SCEP1E6.D01	D3P1.CAL	5.648	8.32	449.70
P2	2048	14.12	1288	4.337	15.867	0.434	SCEP2E6.D01	D3P2.CAL	6.818	10.04	449.60
P3	1365	9.41	1526	3.261	8.521	0.318	SCEP3E6.D01	D3P3.CAL	8.462	12.46	450.00
P4	1040	7.17	1672	2.907	5.742	0.261	SCEP4E6.D01	D3P4.CAL	10.59	15.60	449.70
P5	763	5.26	1631	2.102	3.134	0.193	SCEP5E6.D01	D3P5.CAL	13.39	19.73	449.60
P6	602	4.15	1709	1.757	2.021	0.155	SCEP6E6.D01	D3P6.CAL	15.48	22.80	449.70
P7	652	4.49	1658	1.803	2.175	0.161	SCEP7E6.D01	D3P7.CAL	16.80	24.74	449.30
P8	-----	-----	-----	-----	-----	-----	SCEP8E6.D01	D3P8.CAL	18.78	27.66	449.60
P9	551	3.80	1830	1.735	1.794	0.146	SCEP9E6.D01	D3P9.CAL	21.34	31.44	449.40
P10	4128	28.46	1526	7.525	45.09	0.731	SCEP10E6.D01	D3P10.CAL	4.112	6.72	449.70

* Note: Slant range (R) is derived from the Time of Arrival (T/A) multiplied by the acoustic water velocity (=1473 m/s; based on temperature and salinity measurements).

3.1 Bare Charges

Figure 3 shows a plot of experimental peak pressure versus distance for the uncased charges, together with an exponential line of best fit to the data. Results from the two firings have been averaged and the error bars are smaller than the symbols used to plot the data. It should be noted that records from gauges 6 and 8 have not been used in any of the results presented here, as close examination of the traces from these gauges showed that they were not functioning correctly. The distance of each of the pressure transducers from the centre of the charge was calculated from the time of arrival data and the acoustic water velocity (1473 m/s), which was determined from temperature and salinity measurements. As well as the experimental data Figure 3 also shows pressure values calculated from the similitude equation for the pressure, which has the form [3]

$$P = K\left(\frac{W^{1/3}}{R}\right)^{\alpha} \qquad (1)$$

where P is the pressure in MPa, R the distance in metres, and W the charge mass in kg. For H6 K=59.2 and α=1.19. Figure 3 shows that the experimental peak pressures have the expected exponential decrease with distance, but there is poor agreement with the pressures calculated from equation (1). The difference between the experimental pressures and those calculated from the similitude equation vary from 7% to 10% at the closest distances, to nearly 30% at the position of the furthest gauge. Pressures from the two uncased firings agree to within 2% at each gauge location, and if we take this as an indication of the experimental error then the difference between the experimental values and those calculated from the similitude equation are well outside the limits of experimental error. Equation (1) is only valid in the range from 10.3 MPa to 138 MPa [3] however, and most of our data lies outside this range. Only pressures from the three closest gauges lie within the stated range, and there the differences are on the order of 8%. Although this still lies outside the experimental error, our results lie at the very edge of the region of validity of equation (1), and this may explain the difference.

The energy flux density (EFD) is a measure of the energy carried by the shock wave and is defined by [8];

$$EFD = \frac{1}{\rho_o C_o}\int_o^{5\theta} P^2(t)dt \qquad (2)$$

where ρ_o is the density of water, C_o is the velocity of sound in water, and θ is the time constant, which is defined as the time taken for the peak pressure (P_m) to decay to a value equal to $P_m/2.7183$. The shock wave energy (SWE) at a distance R from the explosive is defined by [8];

$$SWE = 4\pi R^2 \times EFD \qquad (3)$$

and represents the shock energy carried through a spherical surface of radius R centred on the charge. The reduced energy flux density, defined as $EFD/W^{1/3}$, follows a scaling relation of the form [3];

$$EFD/W^{1/3} = K\left(\frac{W^{1/3}}{R}\right)^{\alpha} \qquad (4)$$

For H6 K=115.3, α=2.08, and the relationship is valid in the pressure range from 10.3 MPa to 138 MPa [3]. Figure 4 shows a plot of reduced energy flux density versus distance calculated from the experimental results, as well as values calculated from equation (4). Results for the three gauges closest to the charge show a disagreement of the order of a few percent, but results for the remaining gauges show agreement (within the experimental error of 2%) with the similitude values, even though these experimental values lie outside the range of validity of equation (4).

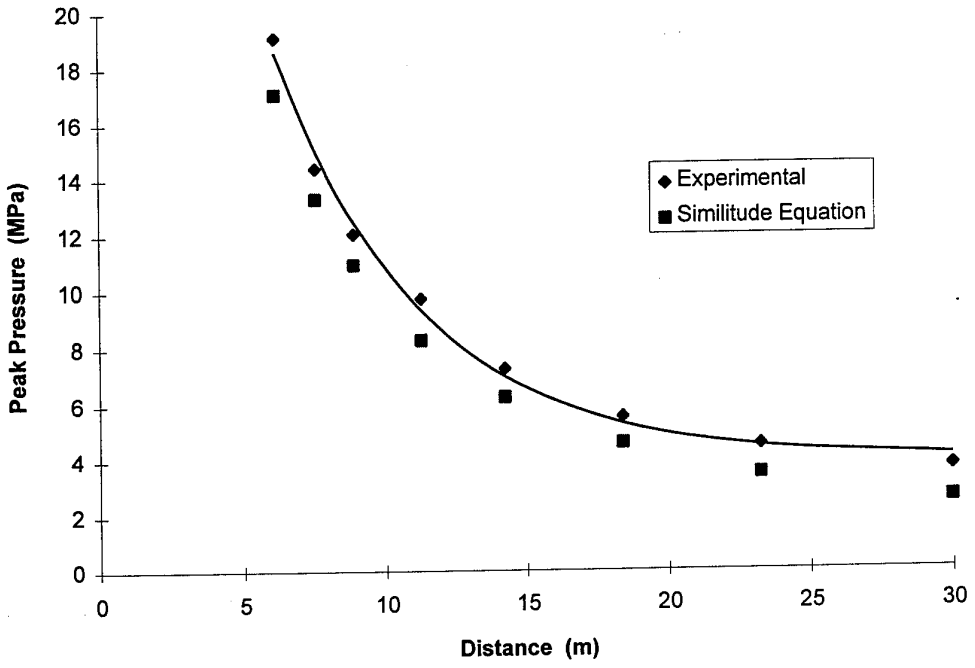

Figure 3: Peak Pressure vs Distance. The solid line is an exponential line of best fit to the experimental data.

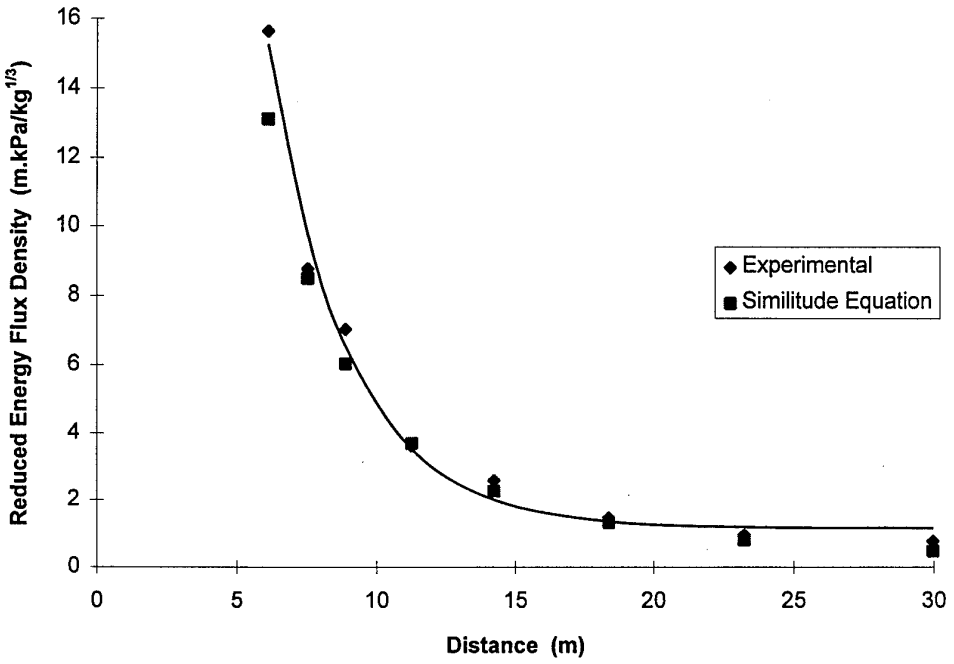

Figure 4: Reduced Energy Flux Density vs Distance. The solid line is an exponential line of best fit to the experimental data.

The first bubble period listed in Tables 1 and 2 is the time interval between the arrival of the first incident shock and the first acoustic signal generated by the hydrostatic compression of the combustion products to the first minimum. There is very little scatter in this data and the values from each of the pressure gauges for both events 1 and 2 agree to within 0.2%, giving an average bubble period for the uncased H6 of 463.5 ms. The bubble period is then used to calculate a bubble period coefficient, defined by [3];

$$K = T\left(\frac{Z^{5/6}}{W^{1/3}}\right) \qquad (5)$$

where T is the first bubble period, K is the bubble period coefficient, W is the charge mass, and Z is the hydrostatic pressure in metres, plus atmospheric pressure (which is approximately equivalent to 10 metres of water). Hence Z=H+10, where H is the charge depth in meters. The relative bubble energy (RBE), which reflects the amount

of work which is done by the expanding combustion products relative to that of some standard charge, is then defined by [8];

$$\text{RBE} = (K_{experimental} / K_{standard})^3 \qquad (6)$$

From equation (5) we calculate K_{H6} = 2.39, and using Pentolite as the standard, for which $K_{Pentolite}$ = 2.11, we calculate a RBE for H6 of 1.46. The value quoted by Swisdack is 1.54, indicating that our value is too low by approximately 5%. Equation (5) is only valid for free water explosions however, where the depths and charge weights are such that the bubble is not closer than about 10 bubble radii to either the surface or bottom. This is not the case here, where the charges were fired at a depth of 8 m in a 16 m deep quarry, and for which the maximum bubble radius is approximately 3 m. Swisdack [3] provides a correction equation relating K and T for cases where either the surface, the bottom, or both, begin to influence the bubble motion. This has the form

$$\frac{0.651\times\phi(y)\times W^{1/3}}{DZ^{1/3}}K^2 - K + \frac{TZ^{5/6}}{W^{1/3}} = 0 \qquad (7)$$

where D is the total depth of water, and y = H/D. For Epping quarry we have y = 0.5, and from [3] we obtain $\phi(y)$ = 0.83. Equation (7) then leads to a revised value for K of K_{H6} = 2.54, which leads to a RBE of 1.76, which is now approximately 14% too high. Bocksteiner [9] has also found a relatively high value for the RBE of PBXW-115 (AUST) using the same main charge and booster configuration as used here. He finds a value of 2.25, compared with the value of 2.00 calculated by Connor [10]. Bocksteiner used a centrally initiated main charge, while Connor used an end initiated system. The centrally initiated system is expected to be more efficient for highly aluminized explosives such as PBXW-115 and H6 because in this case a greater proportion of the gaseous detonation products from the booster will be available to assist the combustion of the main charge. If the RBE for H6 quoted by Swisdack was obtained using an end initiated booster system, as seems to have been prevalent for earlier measurements of this type, then the value obtained here is in good agreeement with previous measurements on H6.

The above analysis of the experimental data for events 1 and 2 indicates that our charges and measurement systems are functioning effectively, and that we are obtaining results for H6 which are in good agreement those reported previously. We now analyse the data from the remaining events to determine the effect of the steel casing on these results.

3.2 Cased Charges

Figure 5 shows a plot of peak pressure versus distance for each of the six charges. There is very good agreement between the measured values at comparable distances for all charges, indicating that the steel casing has negligible effect on peak pressure at these distances (the pressure gauges were located between 6.0 m and 31.6 m from the charge centre). Figure 6 shows the data in somewhat more detail. The pressure values for a given casing thickness have been averaged, and then the percentage change in peak pressure relative to the uncased results have been plotted as a function of distance. The values are scattered randomly about the zero percentage line for both the 6 mm and 12 mm thick cases and no trend towards either an increase or decrease in peak shock pressure is evident.

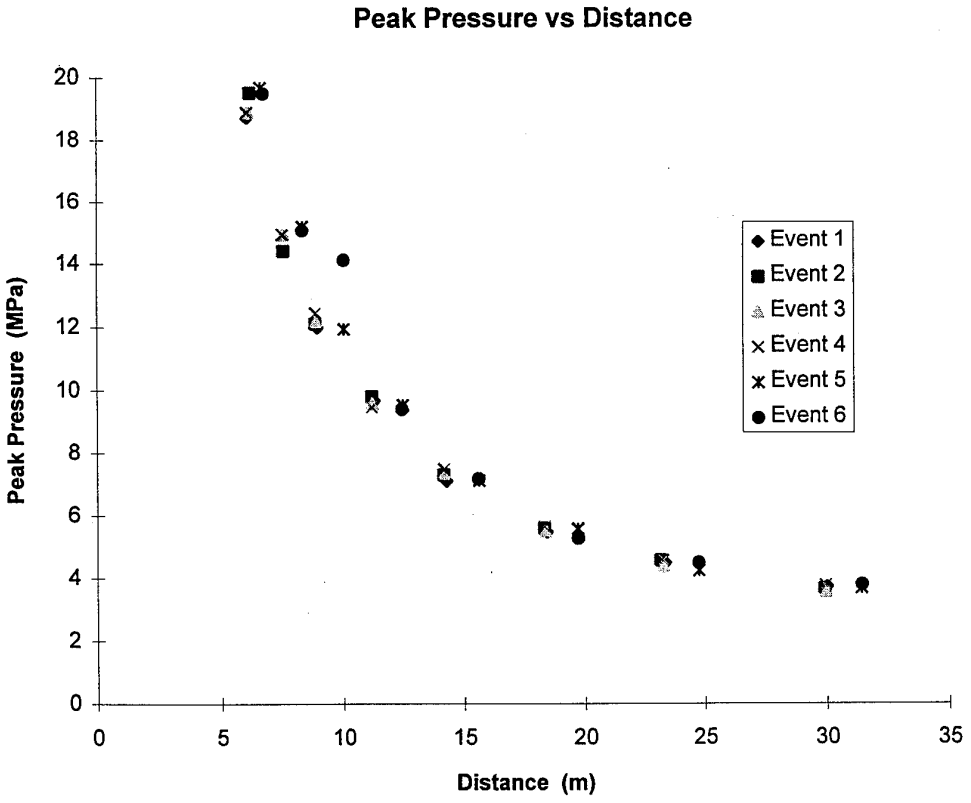

Figure 5: Peak Pressure vs Distance for each of the six charges.

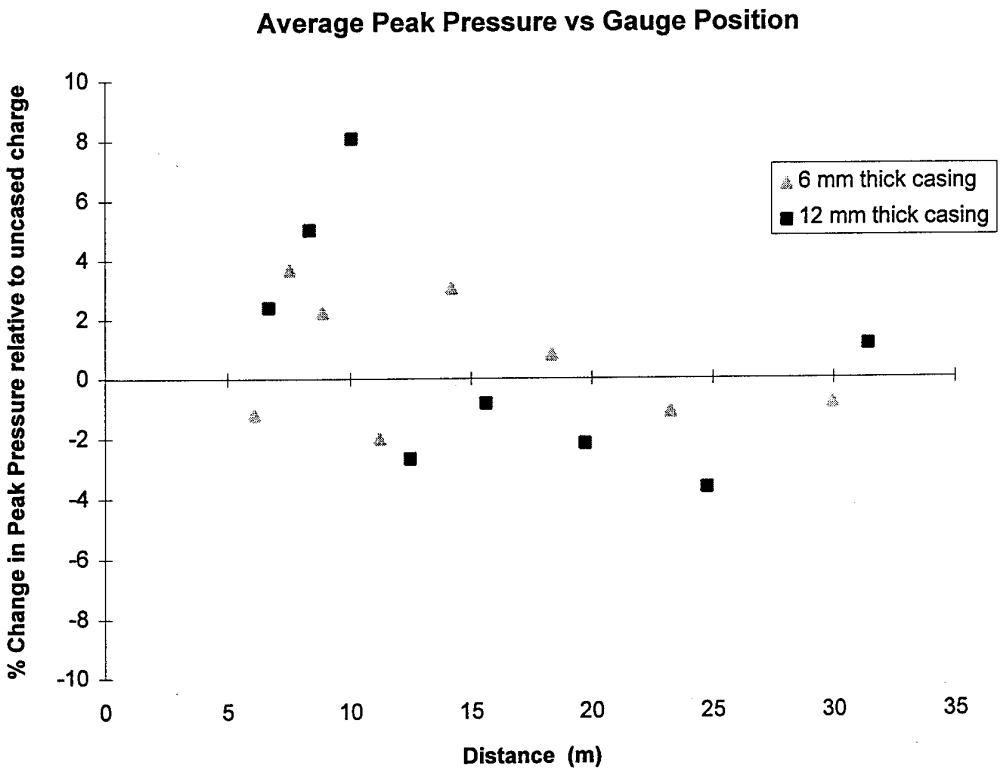

Figure 6: Average Peak Pressure as a function of Distance expressed as percentage relative to uncased charge. Pressure values for the same casing thickness have been averaged.

Whilst the thickness of the casing has no effect on peak pressure it does have a small but noticeable effect on impulse. This is shown qualitatively in Figure 7, which displays a superposition of pressure-time records from gauge number one (at a distance of 8 m) for events 2 and 6 (bare charge and 12 mm thick casing). The solid line is the pressure trace from the bare charge and the dotted line is the trace from the charge with a 12 mm thick case. The slight increase in pulse width shown here is representative of similar results obtained at other gauge locations and will result in a slight increase in both impulse and shock wave energy for a cased charge relative to a bare charge. This is best displayed in quantitative fashion by considering the effect of the casing on the EFD. Figure 8 shows a plot of EFD, calculated from the experimental pressure-time records and equation (2), versus gauge position for the uncased, 6 mm thick, and 12 mm thick cases (the results from similar case thicknesses have been averaged). It would appear from this plot that case thickness has no effect on EFD, but by plotting the results in terms of percentage change in EFD relative to the uncased charge as a function of gauge distance (shown in Figure 9) it becomes clear that the addition of either a 6 mm or 12 mm thick casing does produce an increase in EFD. The

12 mm thick casing results in an average 5% increase in EFD at each gauge location, and the 6 mm thick casing results in an increase of approximatley 7% at around 7 m, decreasing to approximately 2% at 30 m. The effect on the shock wave energy is shown in Figure 10. There is considerable scatter in the data, but a line of best fit through the uncased, 6 mm and 12 mm thick casing results shows that there is a definite trend towards an increase in shock wave energy as the casing thickness increases.

Another important measure of underwater performance is the bubble energy. As discussed in the previous section, this is proportional to the cube of the bubble period. Figure 11 shows a plot of the bubble period for each of the six events determined from each of the pressure gauge records. The bubble period for the uncased charges has an average value of 464 ms, while the results for the 6 mm and 12 mm thick cases are almost indistinguishable and have an average value of 449 ms, indicating that the bubble energy of the cased charges relative to the uncased charge has a value of approximately 0.91.

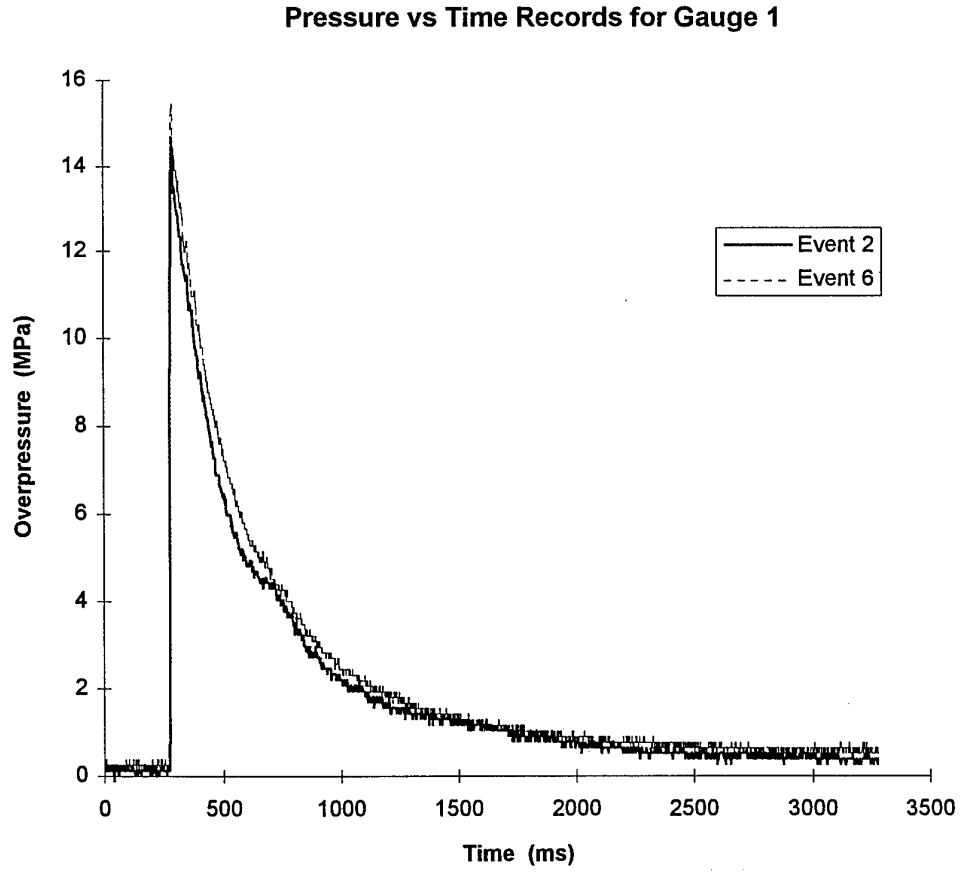

Figure 7: Pressure - Time records from gauge number one (8 m from the charge centre) for events two and six (bare charge and 12 mm thick casing respectively).

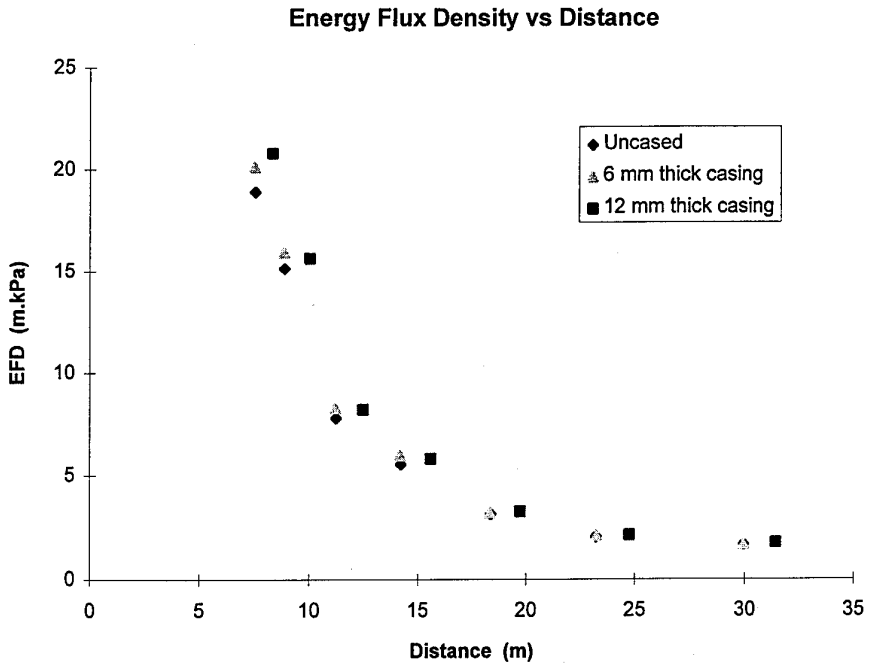

Figure 8: Energy Flux Density vs Distance. EFD values for the same casing thickness have been averaged.

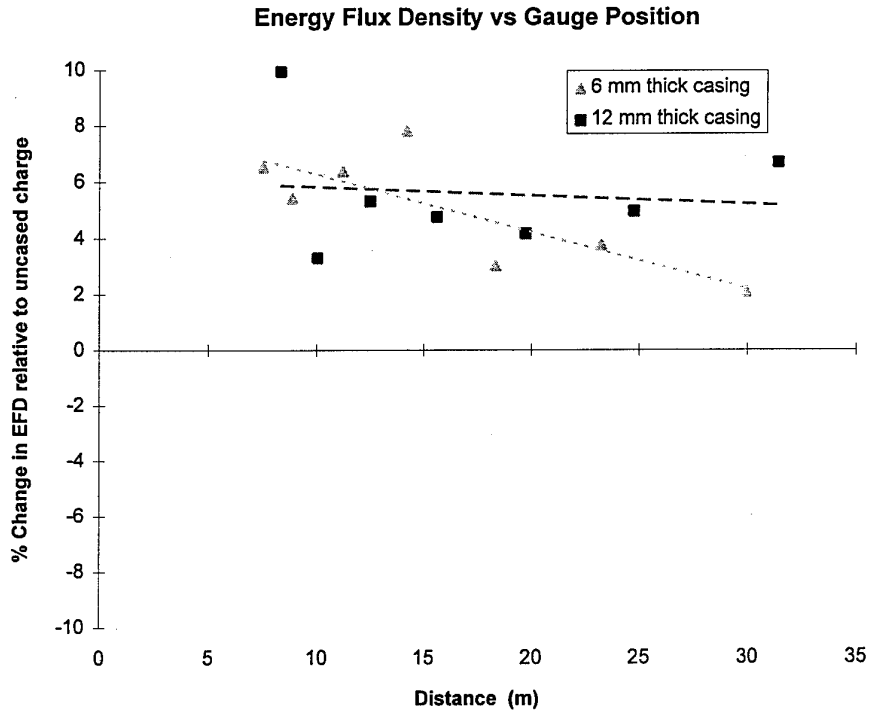

Figure 9: Energy Flux Density as a function of distance expressed as a percentage relative to uncased charge. EFD values for the same casing thickness have been averaged.

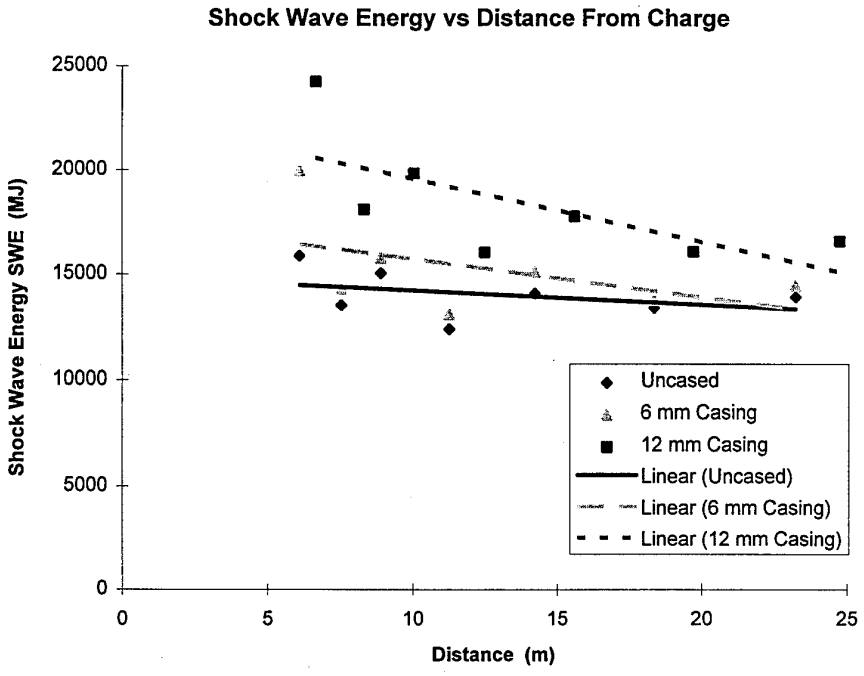

Figure 10: Shock wave Energy for Uncased, 6 mm and 12 mm thick casing. Showing an increase in energy with casing thickness.

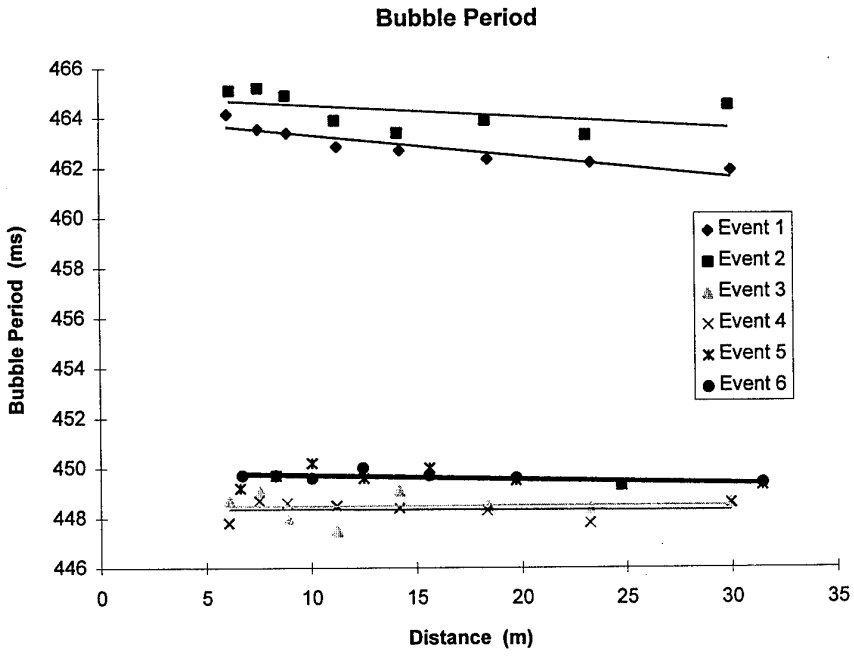

Figure 11: Bubble Period vs Gauge Location for each event determined from experimental records.

4. Numerical Simulations

Our attempts to simulate the main features of the above experimental results and provide some independent confirmation of the effects of case thickness on peak pressure, and relative shock and bubble energy, have stretched the capabilities of the codes available to us to their maximum. The problem is far from simple because of the range of scales involved; the thinnest steel casing has a thickness of only 6 mm, while the furthest gauge is located at a distance of 31.8 m from the charge centre. To resolve the casing implies using computational cells of just a few millimetres in width, and to use cells of this size out to distances of the order of tens of metres is both impractical (because of limitations on the size of arrays in the codes) and unwise (because of accuracy problems). Even though both codes used to model the events had variable griding capabilities the disparity in length scales proved to be the major limitation which prevented us from obtaining results for realistic times and distances.

We began by using Mader's one-dimensional SIN code [11] in spherical geometry to simulate the underwater shock propagation for both bare and cased charges. We had both VAX 8700 and PC versions of the code, but a major limitation of both versions was the restriction to a maximum array size of 999 elements. This meant that we could only follow the shock out to approximately 8 m, and even then the grid was fairly coarse and the peak pressures were in error by approximately 10%. Smoother shock profiles were obtained by focussing attention at much closer distances to the charge, and so simulations were performed for both bare charges and 12 mm thick steel cased charges out to 3 m. The computational details for the runs are provided below, and the results are shown in Figures 12 and 13. The criterion used to determine the time step ensured that it took at least five time steps for the shock to traverse the smallest computational cell. The explosive was initiated by forcing the left hand boundary to move with a designated velocity, and the right hand side of the grid had a flow through boundary condition.

Computational Details for SIN Calculation

Bare Charge

10 cm of H6 at 0.1 cm cell width Burned with C-J volume Burn [11]

Density	1.76 g/cm^3
Pressure$_{C\text{-}J}$	24.0 GPa
Velocity$_{C\text{-}J}$	0.747 cm/μs
Temp$_{C\text{-}J}$	5138 K

Cased Charge

1.2 cm of Steel , 0.2 cm cell width.

Density	7.9 g/cm^3

Both Cased and Uncased

700 cm of Water with cell width varing from 0.25 cm to 1.0 cm

HOM Equation of state for Water

C	0.1483
S	2.0
γ_s	1.0
V_0	1.0
α	0.0001

The results of these simulations are shown in Figure 12, and are in reasonable agreement with the trends shown in the experimental far field results. At distances of 2 and 3 m the shock from the cased charge has a slightly larger impulse than the shock from the uncased charge, and the peak pressures at each location are very similar, with the peak pressure from the cased charge being slightly higher than the pressure from the uncased charge at each of the measurement points. The absolute values of the peak pressures at various near field distances do agree with the extrapolated experimental results, as Figure 13 shows. Although the agreement between simulation and experiment using the SIN code is reasonable, the limitations imposed by the small size of the grid and the one-dimensional geometry were too restrictive, and so we decided to see if better agreement could be obtained with the DYNA2D code.

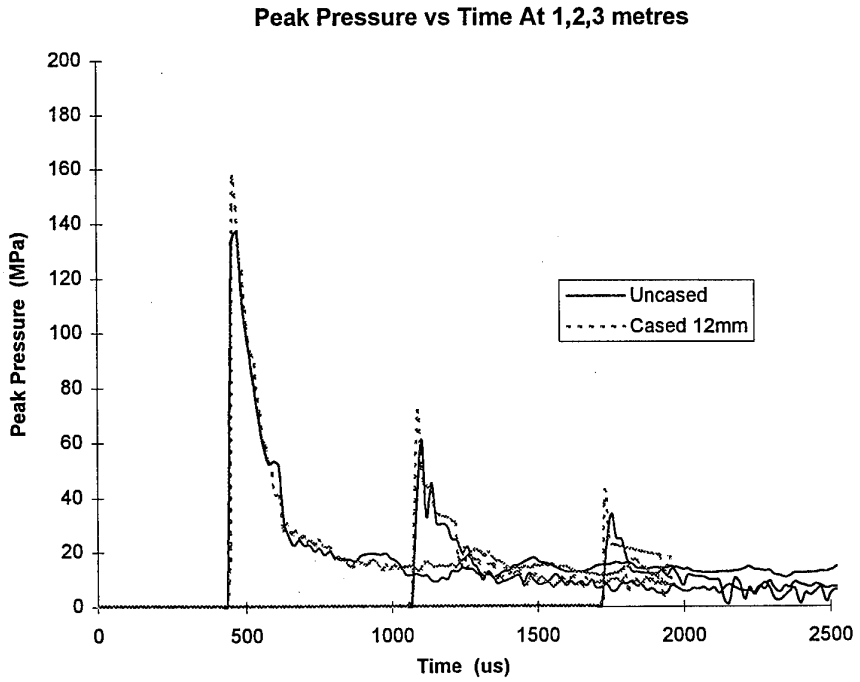

Figure 12: Simulation using SIN. Peak Pressure vs Time at Distances of 1, 2, 3 metres from the charge centre.

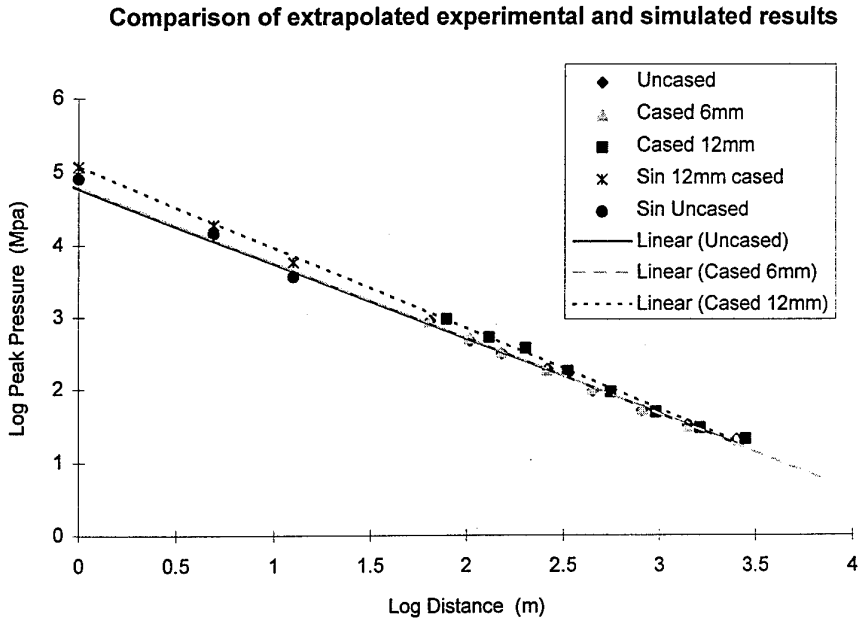

Figure 13: Log Pressure vs Log Distance, Extrapolated Experimental results compared to those from the SIN simulation.

DYNA2D is a two-dimensional finite element code from LLNL [12] and has previously been used to model underwater explosions [13]. We used a PC version of DYNA2D which allowed for a maximum number of approximately 10,000 elements. Even though this is an order of magnitude larger than the number of allowed elements when compared with SIN, the two-dimensional nature of the code requires additional storage arrays and so we found that we were again limited by array sizes, and the maximum distance to which we could carry the computation was again around 8 m. In attempting to perform simulations at these distances we found that the coarse grid resolution resulted in very poor quality pressure-time profiles however, and to get reasonably smooth profiles to enable us to calculate realistic values for impulse and shock wave energy we were forced to perform simulations much closer to the charges than the minimum gauge distance of approximately 6 m. Hence our calculations simulated peak pressures in the range from 0.5 to 1.5 m from the charge, for both bare and cased charges. We used a 25 mm thick steel casing for the DYNA simulations as this allowed us to use a slightly coarser grid, and also ensured that any effects due to the casing would be enhanced.

Using a two-dimensional cylindrical axisymmetric grid meant that only one quarter of the problem had to be modelled. The y-axis was defined to be the axis of symmetry and the x-axis was defined to be totally reflecting, while both the top and right hand edges of the grid were set to model free surface boundary conditions. Slidelines were

placed at the explosive / steel interface, with the steel being the master and the explosive the slave, and also at the steel / water interface, with the water being the slave surface. The explosive was modelled using the JWL equation of state [14] and the detonation was modelled using a programmed burn. The Johnston Cook material model and the Gruneisen equation of state were used to model the steel, and an Isotropic Elastic Plastic-Hydrodynamic material model and Gruneisen equation of state was used to model water.

Computational Details for DYNA Calculation

Bare Charge

10 cm of Explosive H6,

Material parameters (High Explosive Burn)

Density	1.76 g/cm^3
Pressure$_{C\text{-}J}$	24.0 GPa
Velocity$_{C\text{-}J}$	0.747 cm/μs
Temp$_{C\text{-}J}$	5138 K

JWL equation of state

A	7.5807
B	0.08513
R1	4.9
R2	1.1
ω	0.2
E0	0.103

Cased Charge

2.5 cm of Steel , 0.5 cm cell width.

Material parameters (Johnston Cook)

Density	7.9 g/cm^3

Gruneisen equation of state

sp	4.569E-01
s1	1.490E+00
s2	0.000E+00
s3	0.000E+00
γ	2.170E+00

Both Cased and Uncased Charges

700 cm of Water with cell width varing from 0.5 cm to 1.0 cm

Material parameters

Density	1.0
G	0.002
sigy	0.0001
fs	2.0

Gruneisen Equation of state

sp	0.148
s1	2.56
s2	-1.989
s3	0.2268
γ	0.5

The results of the simulations are presented in Figures 14 through 17, which show pressure as a function of time at distances of 50 cm, 75 cm, 100 cm and 150 cm from the charge centre for both bare and cased charges. The figures show that the peak pressure is slightly higher for the uncased charge compared to the cased charge at each of the distances considered, with the maximum difference of approximately 15% occurring at 100 cm. This is consistent with the view that shock impedance effects will alter the peak pressure in the near field, but the differences will tend towards zero in the far field. The "far field" is generally considered to be in the region where the distances from the charge centre are greater than about 10 charge radii, and so the simulation results shown in Figures 14 through 17 actually span the transition region between the near field and far field, where the exact effect of the casing thickness on peak pressure is difficult to predict.

If the profiles in Figures 14 through 17 are normalized so that both the cased and uncased profiles have the same peak pressure, then the impulse from the cased charge is slightly greater than that from the uncased charge at each of the locations considered. We have calculated the impulse from each of these curves by integrating the pressure-time profiles out to 5θ and found that the average increase is 12%, while the experimental value calculated from data at much greater distances from the charge centre is 7%. The discrepancy between these results is probably due to the different casing thickness used in evaluating the experimental results (12 mm) and the simulated results (25 mm), and the fact that the experimental results are evaluated well into the far field, while the simulated results are in the transition region between the near field and the far field.

Unfortunately neither SIN nor DYNA2D could be used to simulate the effect of the case thickness on relative bubble energy. To do this requires running the simulation long enough to follow the expansion of the gas bubble to its maximum radius, followed by the collapse of the bubble to a minimum radius, followed by radiation of the acoustic pulse generated from this collapse out to the position of the furthest pressure transducer. We found that SIN was unable to follow the motion this far because severe distortion of the grid in the neighbourhood of the casing material led to time step problems. DYNA2D was also unable to run the necessary number of time steps because the nature of the boundary condition along one edge of the grid kept reflecting the initial shock back towards the gas bubble. Even if problems of this type could be overcome, further problems remain. In practice, the fragmentation of the steel casing needs to be taken into account, and neither SIN nor DYNA2D can accurately model this process. In DYNA2D the casing could be removed using the interactive rezoning facility, but this would introduce unacceptable errors into the calculation and bring into question the validity of the results. We believe that accurate numerical simulations of the effect of casing thickness on bubble energy would be difficult to achieve using currently available computer codes.

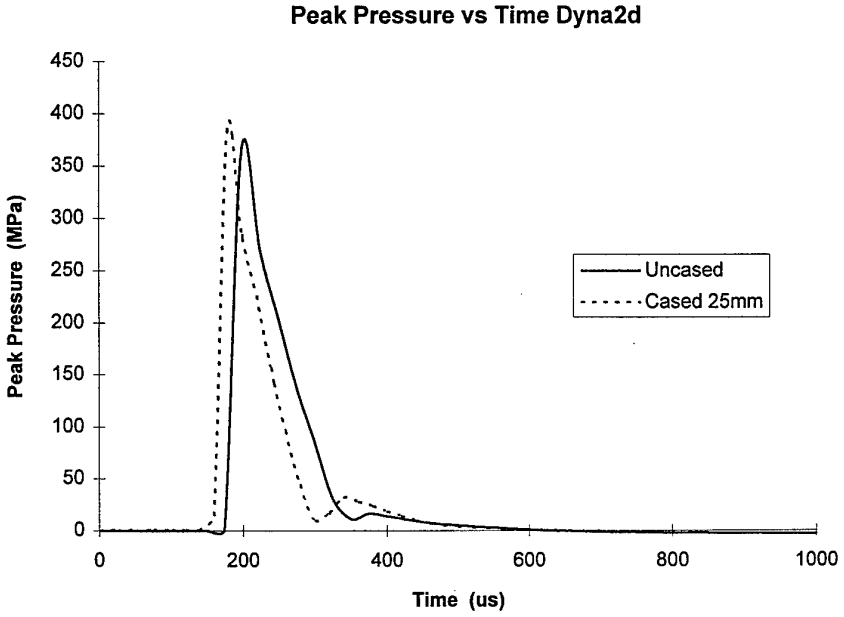

Figure 14: Dyna2d simulation, Peak Pressure vs Time for uncased and 2.5 cm thick cased mines at 50 cm from charge centre.

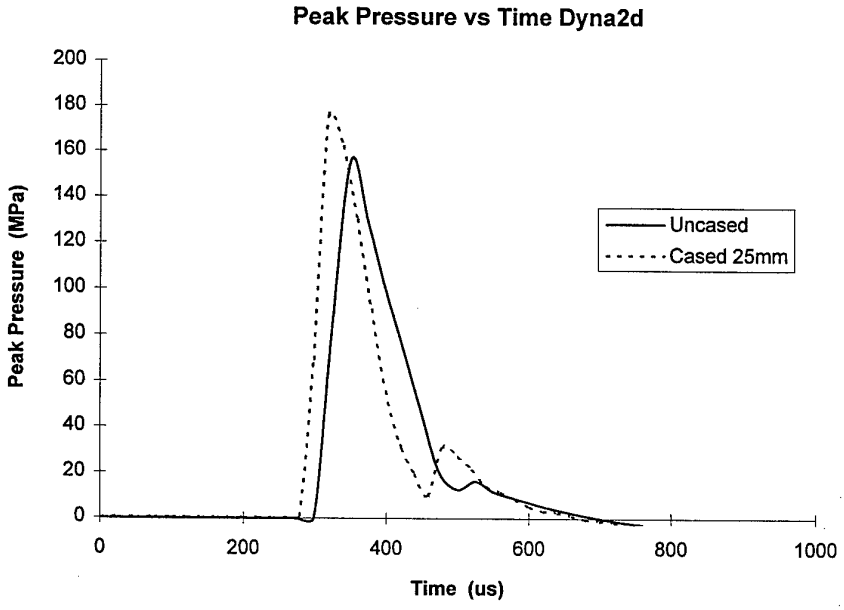

Figure 15: Dyna2d simulation, Peak Pressure vs Time for uncased and 2.5 cm thick cased mines at 75 cm from charge centre.

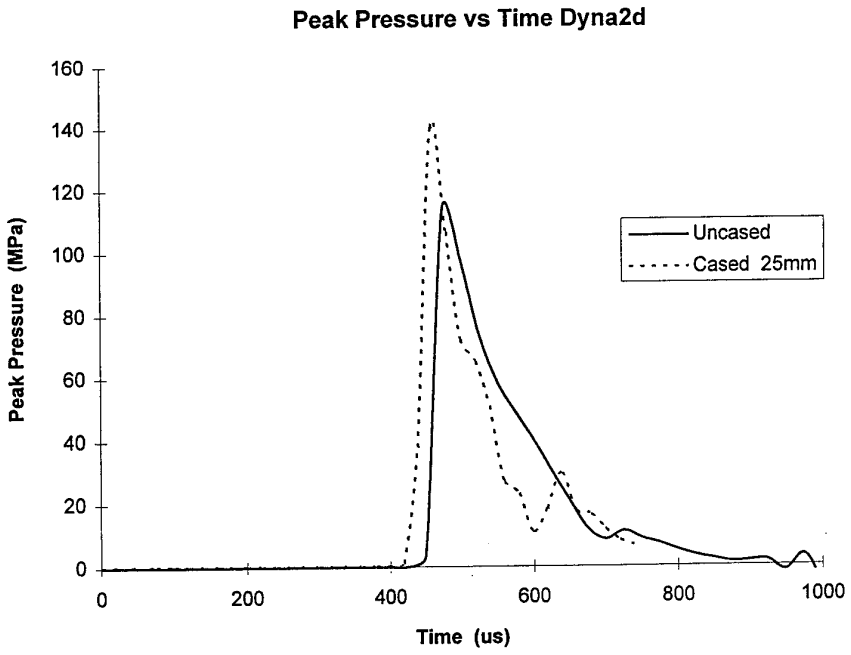

Figure 16: Dyna2d simulation, Peak Pressure vs Time for uncased and 2.5 cm cased mines at 100 cm from charge centre.

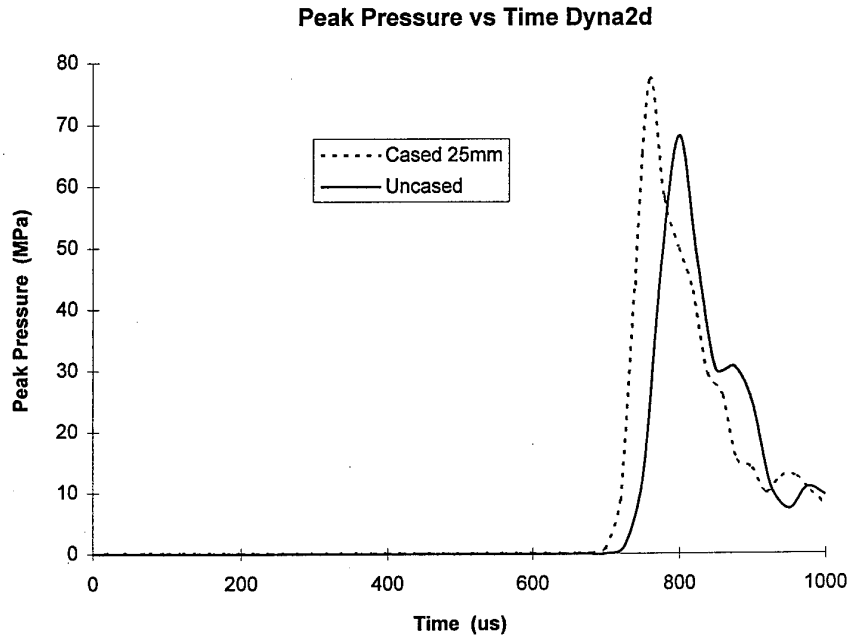

Figure 17: Dyna2d simulation, Peak Pressure vs Time for uncased and 2.5 cm cased mines at 150 cm from charge centre.

5. Discussion and Conclusion

Takahashi et al. [2] have investigated the effect of metal confinement on underwater performance using both experiments and numerical simulations and found results similar to those presented here. They presented their results in terms of the ratio of casing mass to charge mass (M/C) and considered the range from M/C = 2 to M/C = 10. They found that the peak pressure was independent of casing thickness in the far field region, and that the relative shock wave energy increased with the M/C ratio to a maximum value of 1.4 at M/C values of approximately 3, and was then constant for any further increase in M/C ratio. The results presented here for peak pressure and shock wave energy are in agreement with these findings, although our M/C ratios of 0.886 and 1.76 for the 6 mm and 12 mm thick cases are outside the range considered by Takahashi et al.. Our experimental results clearly show that peak pressure is independent of casing thickness in the range from 60 to 300 charge radii, and also show an increase in shock wave energy of approximately 5% for M/C ratios up to 1.87.

There are differences however with regard to the variation of relative bubble energy (RBE) with M/C ratio. Takahashi et al. found experimentally that RBE increased slightly with an increase in M/C ratio. No figures are given, but from their plot it would appear that the increase is no more than a few percent for the range of M/C ratios considered. Our own experimental results show a 9% decrease in RBE for smaller values of M/C ratio. Explaining the difference between these two results is difficult because of a lack of understanding of the many processes which occur at the explosive/water or explosive/metal/water interface. Shepherd [15] has discussed some of these effects in detail and notes that the bubble period can be affected by evaporation of superheated water created by shock heating and bubble expansion during oscillation. This effect is most important at small depths (ie. 100 m or less), and for explosives with nonideal behaviour will be scale dependent. It should be noted that our own experiments used 10 kg charges of H6 fired at 8 m depths, while those of Takahashi et al. were 0.5 kg charges of RDX/polyurethane binder (75:25) fired at 4 m depth. A complete understanding of this process would also require consideration of the turbulent flow created at the boundary, which would greatly enhance the mixing of evaporated water vapour with the explosion products. A detailed study would require accurate simulations of case fragmentation and modelling of the multiphase region created by heat transfer from the shock heated fragments into the surrounding water and products. Such a study is beyond the scope of the present report.

The results presented here and in the paper by Takahashi et al. indicate that for damage mechanisms due to peak pressure or shock wave energy the relatively thick casing of the Mk 80 series of bombs will not result in any degradation of performance, and may even result in enhanced damage due to shock wave effects. The situation with regard to damage by bubble effects is less clear, and may at worst result in a 9% reduction in performance, independent of M/C ratio.

6. Acknowledgements

We thank M. Chick for several discussions and assistance during the early planning stages of this work, G. Bocksteiner and G.Yiannakopoulos for advice on underwater effects and analysis of the data, and D. McQueen, A. Krelle, F. Marion and A. Pleckauskas for the successful conduct of the trials. We also thank Warren Reid for providing calculations on the fragmentation hazard of the cased charges

7. References

1. R.H Cole, (1948) "Underwater Explosions", Dover Publications, New York.

2. K. Takahashi, K. Murata and Y. Kato, "Underwater Shock Enhancement by Metal Confinement", 13th International Symposium on Ballistics, Stockholm, Sweden, June 1992, pp. 531-538.

3. Swisdak, M.M., "Explosion Effects and Properties: Part 2-Explosion Effects in Water", NSWC/WOL TR 76-116, 1978

4. Hyde, D.W. (1990) "CONWEP - Conventional Weapons Effects Computer Program", U.S. Army Corps of Engineers.

5. Warren Reid, personal communication, February 1992.

6. Best, J. " Fortran computer program for computing gas bubble data for underwater explosions", MRL VAX 8700 Computer System.

7. Jenks G.J., Masinskas J.J. and Oliver J.D., "Trajectories of Fragments from Detonating Munitions", MRL Technical Note 264, February 1974.

8. Roth, J. (1983) "Underwater Explosives", in: Encyclopedia of Explosives and Related Items, Vol 10, US Army Research and Development Command, Dover, New Jersey, pp. U38-U81.

9. Bocksteiner, G. "Evaluation of Underwater Explosive Performance of PBXW-115 (AUST)", AMRL Technical Report, in preparation, file number 510/207/0198.

10. Connor, J.G. (1984) "Underwater Explosion Effectiveness of PBXW-113, PBXW-114 and PBXW-115", Naval Surface Warfare Center Technical Report, NSWC-TR 84-396.

11. Mader, C.L. (1979) "Numerical Modelling of Detonations". University of California Press.

12. Hallquist, J.O. (1984). "User's manual for DYNA2D - an explicit two-dimensional hydrodynamic finite element code with interactive rezoning", UCID - 18756, Rev. 2, Lawrence Livermore National Laboratory, Ca., USA.

13. Miller, P.J. and Guirguis, R.H. (1993) "Experimental Study and Model Calculations of Metal Combustion inAl/AP Underwater Explosives", Mat. Res. Soc. Symp. Proc., 296, 299 - 304.

14. Kurry, J.W., Hornig, H.C., Lee, E.L., McDonnel, J.L., Ornellas, D.L., Finger, F., Strange, F.M., and Wilkins, M.L. (1966) "Metal Acceleration be Chemical Explosives", Fourth Symposium (International) on Detonation, Office of Naval Research, ACR-126, Washington, DC.

15. Shepherd, J.E. (1988) "Interface Effects in Underwater Explosions", Office of Naval Research Workshop Report on Conventional Weapons Underwater Explosions, pp 43 - 83, prepared by Georgia Institute of Technology, Atlanta, Georgia.

SECURITY CLASSIFICATION OF THIS PAGE **UNCLASSIFIED**

REPORT NO.	AR NO.	REPORT SECURITY CLASSIFICATION
DSTO-TR-0120	AR-009-172	UNCLASSIFIED

TITLE

Effects of case thickness on the performance of underwater mines

AUTHOR(S)
D.A. Jones and E.D. Northeast

CORPORATE AUTHOR
DSTO Aeronautical and Maritime Research Laboratory
GPO Box 4331
Melbourne Victoria 3001

REPORT DATE	TASK NO.	SPONSOR
January 1995	NAV 92/301	DNMOP

FILE NO.	REFERENCES	PAGES
510/207/0153	14	32

CLASSIFICATION/LIMITATION REVIEW DATE

CLASSIFICATION/RELEASE AUTHORITY
Chief, Weapons Systems Division

SECONDARY DISTRIBUTION

Approved for public release

ANNOUNCEMENT

Announcement of this report is unlimited

KEYWORDS

Naval mines	Bubble chambers	Explosives
Transducers	Fabrication	Explosive charges
Thickness	Numerical simulation	Case depth

ABSTRACT

The effect of case thickness on the performance of underwater mines was investigated both experimentally and computationally using 10 kg charges of H6. The charges were cylindrical in shape and surrounded by either 6 mm or 12 mm thick steel casing. Two bare charges were also fired. Analysis of the experimental pressure transducer records showed that casing thickness had no effect on peak pressure in the far field, but resulted in a 5% increase in shock wave energy compared with an uncased charge. Numerical simulations using both the SIN and DYNA2D codes supported these experimental results. Measurements of the bubble period indicated that the bubble energy for a cased charge was 9% lower than that of an uncased charge.

Effects of Case Thickness on the Performance of Underwater Mines

D.A. Jones and E.D. Northeast

(DSTO-TR-0120)

DISTRIBUTION LIST

Director, AMRL
Chief, Weapons Systems Division
Dr B.W. Thorpe
Dr D.A. Jones
Mr E.D. Northeast
Library, AMRL Maribyrnong
Library, AMRL Fishermens Bend

Chief Defence Scientist (for CDS, FASSP, ASSCM) — 1 copy only
Director, ESRL
Head, Information Centre, Defence Intelligence Organisation
OIC Technical Reports Centre, Defence Central Library
Officer in Charge, Document Exchange Centre — 8 copies
Navy Scientific Adviser
Air Force Scientific Adviser, Russell Offices
Scientific Adviser - Policy and Command
Senior Librarian, Main Library DSTOS
Librarian, DSD, Kingston ACT
Serials Section (M List), Deakin University Library, Deakin University, Geelong 3217
NAPOC QWG Engineer NBCD c/- DENGRS-A, HQ Engineer Centre, Liverpool Military Area, NSW 2174
ABCA, Russell Offices, Canberra ACT 2600 — 4 copies
Librarian, Australian Defence Force Academy
Head of Staff, British Defence Research and Supply Staff (Australia)
NASA Senior Scientific Representative in Australia
INSPEC: Acquisitions Section Institution of Electrical Engineers
Head Librarian, Australian Nuclear Science and Technology Organisation
Senior Librarian, Hargrave Library, Monash University
Library - Exchange Desk, National Institute of Standards and Technology, US
Acquisition Unit (DSC-EO/GO), British Library, Boston Spa, Wetherby, Yorkshire LS23 7BQ, England
Library, Chemical Abstracts Reference Service
Engineering Societies Library, US
Documents Librarian, The Center for Research Libraries, US
Army Scientific Adviser, Russell Offices - data sheet only
Director General Force Development (Land) - data sheet only
DASD, APW2-1-OA2, Anzac Park West, Canberra ACT - data sheet only
SO (Science), HQ 1 Division, Milpo, Enoggera, Qld 4057 - data sheet only
Librarian - AMRL Sydney - data sheet only
Counsellor, Defence Science, Embassy of Australia - data sheet only
Counsellor, Defence Science, Australian High Commission - data sheet only
Scientific Adviser to DSTC Malaysia, c/- Defence Adviser - data sheet only
Scientific Adviser to MRDC Thailand, c/- Defence Attache - data sheet only

Dr R. Spear, WSD
Mr M.C. Chick, WSD
Mr G. Bocksteiner, WSD
Dr D.J. Whelan, WSD
LCDR S. McCarey, SOMCD, MHQ, Wylde St, Potts Point, Sydney NSW 2001